Dark matter at the end of the Galaxy

Mariangela Lisanti, Louis E. Strigari, Jay G. Wacker, and Risa H. Wechsler

Phys. Rev. D **83**, 023519 — Published 24 January 2011

DOI: 10.1103/PhysRevD.83.023519

The Dark Matter at the End of the Galaxy

Mariangela Lisanti,[1,2] Louis E. Strigari,[3] Jay G. Wacker,[2] and Risa H. Wechsler[2,3]

[1]*PCTS, Princeton University, Princeton, NJ 08540*
[2]*Particle & Particle Astrophysics Department, SLAC National Accelerator Laboratory, Menlo Park, CA 94025*
[3]*Kavli Institute for Particle Astrophysics and Cosmology & Physics Department, Stanford University, Stanford, CA 94305*

Dark matter density profiles based upon ΛCDM cosmology motivate an *ansatz* velocity distribution function with fewer high velocity particles than the Maxwell-Boltzmann distribution or proposed variants. The high velocity tail of the distribution is determined by the outer slope of the dark matter halo – the large radius behavior of the Galactic dark matter density. N-body simulations of Galactic halos reproduce the high velocity behavior of this *ansatz*. Predictions for direct detection rates are dramatically affected for models where the threshold scattering velocity is within 30% of the escape velocity.

I. INTRODUCTION

Dark matter is the dominant form of matter in the Universe and measuring its properties is one of the most important outstanding problems in astrophysics and particle physics. Directly detecting Galactic dark matter through terrestrial experiments is probably the least ambiguous method for determining its identity. Accurately predicting scattering rates for direct detection experiments requires a model for the velocity distribution of Galactic dark matter. This article proposes a class of velocity distribution functions that are motivated by cosmological models for the Galactic dark matter and studies how this *ansatz* affects predictions for direct detection experiments.

Dark matter halos form through a continuous process of smooth accretion and merging of smaller mass halos in the ΛCDM model of cosmology. Clues about the formation history of these halos can be found in their phase space distributions, motivating a careful study of dark matter densities and velocities. Modern numerical simulations, which probe a large range of halo mass scales, have shown that the merging process leads to a near universal double-power-law density profile that is approximately described by the Navarro-Frenk-White (NFW) model [1]. Though the physical origin for NFW-like profiles is unknown, they provide a valuable link between the small scale properties of dark matter halos and the cosmological model on large scales.

The velocity distribution is dynamically related to the density profile for equilibrium dark matter halos [2, 3]. In direct dark matter detection studies, the 'Standard Halo Model' (SHM) [4] is the canonical velocity distribution for interpreting results from experiments and constraining dark matter models [5]. Isothermal and isotropic approximations to the dark matter distribution functions such as the SHM are useful because they simplify rate calculations. However, recent high resolution cosmological simulations provide strong evidence that the SHM does not appropriately capture the behavior of the dark matter in the Galactic halo [6–9]. By mapping out the dark matter phase space distribution, these N-body simulations consistently point to deviations from a standard Maxwellian velocity distribution function, most prominently at the tail of the distribution [10]. This new evidence motivates a reevaluation of the SHM and careful consideration of velocity distributions that better capture the features of the Galactic halo.

There have been recent attempts to derive the dark matter velocity distribution from first principles [11] or from observations of rotation curves [12]. However, the resulting models over-predict the number of high velocity particles compared to the highest resolution dark matter-only numerical simulations with $\sim 10^3$ $M_\odot$ particles [6, 7], as well as simulations that include baryons [8]. It has been claimed that Tsallis distributions, derived from non-extensive statistical mechanics [13], provide a good fit for the baryon plus dark matter simulation in [8]. However, because the resolution for this simulation is $\sim 7 \times 10^5$ $M_\odot$, it is limited at probing the high velocity tail relative to the dark matter only simulations. An alternate approach is to fit the numerical results with an arbitrary function [7, 9]; while these models are useful for making experimental predictions, there is no clear motivation for the fit parameters.

This paper obtains a velocity distribution function that describes the double power-law density models. While these velocity distributions have been obtained numerically for isotropic models and also for certain classes of spherical anisotropic models [14–16], no analytic solution has been found. The isotropic velocity distribution function corresponding to double power-law density profiles [1] is described by

$$f_k(v) \propto \left[\exp\left(\frac{v_{\rm esc}^2 - v^2}{k\, v_0^2}\right) - 1\right]^k \Theta(v_{\rm esc} - v), \quad (1)$$

where k is the power-law index, $v_{\rm esc}$ is the escape velocity, and v_0 is the dispersion. This distribution function is significantly different from Maxwell-Boltzmann distributions and its variants in the high velocity tail. It describes only the smooth dark matter component; modifications to the distribution function from discrete subhalos and streams can be important phenomenologically but need to be added separately [17–19]. Additionally, deviations from a smooth distribution arise from gravitational scattering from the Sun and the Jovian planets [20].

Direct dark matter detection experiments look for low energy nuclear recoil events caused by dark matter scattering off of target nuclei [21]. The nuclear recoil thresholds for dark matter detection experiments are in the range of tens of keV, which implies that the recoil energies in many models of dark matter are well below threshold. Only particles with the largest velocities have sufficiently energetic nuclear recoils to be visible at direct detection experiments. This fact makes it particularly important to accurately describe the high velocity tail of the dark matter velocity distribution in the halo surrounding the Milky Way. Relative to a Maxwell distribution, (1) predicts a smaller fraction of dark matter near the escape velocity, which affects the relative rates between direct detection experiments, especially those with different target nuclei or energy thresholds.

This paper is organized as follows. Sec. II motivates the *ansatz* in (1) and derives a general form for the power-law index. Sec. III compares (1) to numerical calculations of the full velocity distribution function for Milky Way-like spatial profiles, including a gravitational potential model of the disk. The ansatz in (1) is also compared to the results of N-body simulations. Elementary direct detection phenomenology is explored in Sec. IV, and conclusions are presented in Sec. V.

II. EQUILIBRIUM DARK MATTER DISTRIBUTIONS

The Galactic halo forms through a process of hierarchical merging, smooth accretion, and violent relaxation [1, 22, 23]. The central regions of halos, where relaxation processes have ended, are in quasi-static equilibrium [24]. In this case the dominant component of Galactic dark matter is described by a steady-state distribution function that evolves slowly with time. In the outer regions of the halo, at low binding energies, the phase space distribution will depend more dramatically on both the history and environment of the halo. For example, a halo with a fairly quiescent formation history will have a different phase space distribution at low binding energies compared to one with a recent major merger [6]. Sec. III argues that the behavior of the distribution function of the Milky Way at high velocities and low binding energies resembles an equilibrated system on average. There can be large excursions from equilibrium at the high velocity tail due to recent accretion; however, N-body simulations suggest that these are spatially localized streams.

According to Jeans theorem, the six-dimensional phase space distribution function $f(\vec{x}, \vec{v})$ for a spherically symmetric and isotropic system can be written in terms of the energy, which is an integral of motion:

$$\mathcal{E} \propto 2\psi(\vec{x}) - \vec{v}^2. \tag{2}$$

The local escape velocity is defined as the velocity where $\mathcal{E} = 0$ and therefore

$$\mathcal{E} \propto v_{\rm esc}^2(r) - v^2. \tag{3}$$

Due to the assumption of equilibrium, $f(\mathcal{E})$ for $\mathcal{E} < 0$ must vanish since this corresponds to particles with velocities greater than the escape velocity of the system.

If the dark matter of the Milky Way is nearly equilibrated, then the Jeans theorem implies that the dark matter density determines the velocity distribution function. Dark matter halos in cosmological simulations are well fit by spherically averaged double power-law density distributions of the form,

$$\rho(r) = \frac{\rho_s}{(r/r_s)^\alpha (1 + (r/r_s))^{(\gamma-\alpha)}}, \tag{4}$$

where ρ_s is the scale density, r_s is the scale radius, α is the slope of the halo density near the core, and γ is the slope at large radii. For example the NFW profile has $(\alpha, \gamma) = (1, 3)$ [1], while the Hernquist model has $(\alpha, \gamma) = (1, 4)$ [25]. The Jaffe model has $(\alpha, \gamma) = (2, 4)$, but the $\alpha = 2$ inner slope is steeper than indicated by numerical simulations.

Velocity distribution functions that behave as Maxwell-Boltzmann distribution functions at low velocities arise from dark matter halos with inner slopes of $\alpha = 2$. This article is primarily concerned with the effects of the dark matter velocity distribution on direct detection rates. The relative velocity between dark matter and target nuclei for $v \ll v_0$ is set by the solar velocity; therefore, the low velocity behavior of the Galactic dark matter does not significantly affect direct detection rates. Though finding a velocity distribution function that describes $\alpha < 2$ is important, these modifications to the dark matter velocity do not qualitatively change the direct detection rates [26]. The goal of this section is to derive a phenomenological velocity distribution function that can arise from these double power-law density models to predict direct dark matter detection rates.

A given density distribution is related to the velocity distribution through the gravitational potential of the halo, $\psi(r)$:

$$\nabla^2 \psi = -4\pi G\rho = -4\pi G M \int f(v) d^3v, \tag{5}$$

where G is the gravitational constant and M is the halo mass. For an isotropic density distribution, there is a one-to-one correspondence between the density and ergodic distribution function, given by the Eddington formula:

$$f(\psi) = \frac{1}{\sqrt{8}\pi^2}\left[\int_0^\psi \frac{d\psi'}{\sqrt{\psi - \psi'}} \frac{d^2\rho}{d\psi'^2} + \frac{1}{\sqrt{\psi}}\Big(\frac{d\rho}{d\psi}\Big)_{\psi=0}\right]. \tag{6}$$

The expression for $f(\psi)$ can be written in terms of the binding energy $\mathcal{E}$ by replacing $\psi \to \mathcal{E}$. Equation (6) is a powerful simplification that allows one to solve for the distribution function of an arbitrary spherical density model. In many cases, however, the solution for $f(v)$ is

analytically intractable and must be obtained by solving (6) numerically. This is the case for most combinations of (α, γ) in (4); as a result, there is no general closed-form analytic solution for the velocity distribution function that corresponds to double power-law density models. Fortunately, it is still possible to assume an *ansatz* for $f(v)$ that reproduces the numerical solution of the Eddington formula for double power-law densities. The possibilities for such an *ansatz* are limited if one assumes that the dark matter halo is in equilibrium.

The high velocity tail of the local dark matter distribution function arising from equilibrated, double power-law models is in conflict with the Standard Halo Model and its variants. Consider the following generalization of the Standard Halo Model as an *ansatz*

$$f(\mathcal{E}) \propto (e^{\mathcal{E}/\mathcal{E}_0} - 1)^k \Theta(\mathcal{E}), \tag{7}$$

where k is the power-law index of the distribution and describes the behavior near the escape velocity. The benefit of this *ansatz* is that it satisfies the Jeans theorem for an equilibrated system and goes continuously to zero at the escape velocity.

The power-law index is defined as

$$k = \lim_{\mathcal{E} \to 0^+} k(\mathcal{E}), \tag{8}$$

with

$$k(\mathcal{E}) \equiv \frac{\mathcal{E}}{f(\mathcal{E})} \frac{df(\mathcal{E})}{d\mathcal{E}}. \tag{9}$$

For double-power density profiles of the form in (4), the power-law index can be evaluated analytically. In this case, the second term of the Eddington formula is negligible. Expanding the density, potential, and the distribution function in (6) around small $\mathcal{E}$ gives a power-law index

$$k = \gamma - \frac{3}{2} \tag{10}$$

for $\gamma > 3$ [27]. As $\gamma \to 3$, $k(\mathcal{E})$ does not approach a simple power-law and the approximations that lead to (10) break down [14]. Sec. III fits the numerical solutions to the parameters for the *ansatz* velocity distribution function in (1). As $\gamma \to 3$, the best fits for k tend to be $k \simeq 2.0$, slightly larger than (10). Earlier studies from galaxy formation via violent relaxation motivated $k = 1.5$ [28].

It is remarkable that k takes such a general and simple form. The index is determined almost exclusively by the outer slope of the density distribution; all terms that depend on α vanish in the low energy limit. The outer slope controls the behavior of k because the dark matter particles with the highest velocities are those with the smallest binding energies. These particles will be in highly energetic orbits about the halo, and will be concentrated at large radii, far from the core. Density distributions with larger outer slopes have fewer particles orbiting at large radii, which means that the low-energy component of $f(\mathcal{E})$ is suppressed. A large value of k precisely captures this behavior.

The distribution function for binding energies can be rewritten in terms of velocities using the relation in (3) to get (1). The velocity distribution *ansatz* in (1) is well-described by a Gaussian peaked near v_0 for $v \ll v_{\rm esc}$. As $v \to v_{\rm esc}$, the distribution function approaches

$$f(v) \to (v_{\rm esc} - v)^k. \tag{11}$$

Cosmological N-body simulations indicate $\gamma \sim 3 - 5$ [1, 29], which means that the velocity distribution falls off near the escape velocity to the power $k = [1.5, 3.5]$. A more detailed comparison with cosmological simulations follows in Sec. III.

The Standard Halo Model and the King model provide a useful comparison to the distribution in (7) and they are defined, respectively, as

$$\begin{aligned} f_{\rm SHM}(\mathcal{E}) &= N(\mathcal{E}_0) e^{\mathcal{E}/\mathcal{E}_0} \Theta(\mathcal{E}) \\ f_{\rm King}(\mathcal{E}) &= N(\mathcal{E}_0)(e^{\mathcal{E}/\mathcal{E}_0} - 1)\Theta(\mathcal{E}). \end{aligned} \tag{12}$$

These distributions are frequently used for direct dark matter detection predictions because they make the calculations tractable. In addition, they satisfy Jeans theorem under the assumption of isotropy and spherical symmetry. However, they do not correspond to NFW-like density models, especially near the high-velocity tails of the distributions. In particular, the SHM behaves near the tail as $k \to 0$, and the King model has $k = 1$. Consequently, these velocity distribution functions over-predict the number of particles in the tail of the distribution.

The Tsallis distribution is another model for the velocity distribution that has been recently discussed in the literature, and is defined as

$$f_{\rm Tsallis}(v) \propto \left(1 - (1-q)\frac{v^2}{v_0^2}\right)^{q/(1-q)}. \tag{13}$$

The Tsallis distribution predicts that the escape velocity is given by $v_{\rm esc}^2 = v_0^2/(1-q)$ and $k = q/(1-q)$, where the distribution in (1) sets these three parameters independently. Hansen et al. [30] show there is a correlation between the parameter q and the local density slope, implying that q varies with radius if the density slope is not the same at all radii. A disadvantage of this model, however, is that does not satisfy the Jeans theorem for spherical and isotropic systems if the circular velocity, v_0, is held constant. This violation of Jeans theorem is also true for the generalized Maxwellian distribution, which has been used to model the radial and tangential components of the velocity distribution [9].

The formalism and models in this section only apply to the spherically-averaged velocity distribution, and do not capture any physics pertaining to steams, subhalos, or any other structure in the phase space distribution. Though streams are unlikely to affect the overall velocity distribution because their densities are less than $\sim 0.1\%$

of the smooth dark matter density [6], they are seen to occupy the high energy tail of the velocity distribution [17, 31].

III. NUMERICAL EVALUATION

The previous section derived how the high velocity tail of the dark matter phase space is populated for cosmologically-motivated spatial densities. The *ansatz* in (1) interpolates between a Maxwellian distribution at low velocities to one matching the high velocity behavior in (10). This section compares the analytic approximation in (10) with the velocity distributions that are calculated from the full numerical solution of the Eddington formula in (6). Additionally, it shows that the *ansatz* distribution function accurately describes the velocity distributions of simulated dark matter halos both with and without baryonic physics.

A. Distribution Function Model for the Milky Way

A full gravitational potential model for the Milky Way is necessary to evaluate the Eddington formula, which requires including a model for the baryons. The potential model is comprised of the sum of three components: the dark matter, the disk, and the bulge, so that $\psi_{\rm tot} = \psi_{\rm halo} + \psi_{\rm disk} + \psi_{\rm bulge}$. The halo mass within a given radius is obtained from (4), while the velocity of the local standard of rest (LSR) and the escape velocity are given by

$$v_{\rm lsr}^2 = -r\frac{d\psi_{\rm tot}}{dr} \qquad v_{\rm esc} = \sqrt{2|\psi_{\rm tot}|}, \tag{14}$$

respectively.

The value of $\psi_{\rm halo}$ is uniquely determined for a given pair, (α,γ), and for specific values of the scale radius, r_s, and scale density, ρ_s. The velocity distribution *ansatz* in (1) is compatible with any value of the outer slope with $\gamma > 3$, while the inner slope is given by $\alpha = 2$. However, the behavior of the potential for $r \ll r_s$ dominantly determines the low velocity behavior of Galactic dark matter and does not significantly affect predictions for direct detection rates.

The full model for $\psi_{\rm total}$ needs to include additional potentials for the bulge and disk components. Here, a spherically-symmetric potential is used for the bulge component of the form

$$\psi_{\rm bulge} = -GM_{\rm bulge}/r, \tag{15}$$

where the mass of the bulge is $M_{\rm bulge} = 10^{10}\,M_\odot$ [3]. The disk is modeled by a spherical potential of the form

$$\psi_{\rm disk} = -GM_{\rm disk}(1 - e^{-r/r_d})/r. \tag{16}$$

The potential formula in (16) contributes ~ 115 km s^{-1} to the circular velocity for a disk consisting of gas and stars with $M_{\rm disk} = 5 \times 10^{10}$ M$_\odot$ and a scale length of $r_d = 5$ kpc. The spherical approximation in (16) is the monopole term for a standard axisymmetric double exponential disk potential [3]. In comparison, for the assumed disk mass, the axisymmetric double exponential disk potential gives $v_{\rm lsr} \simeq 130$ km s^{-1} at the solar radius, and is 11% larger than $v_{\rm lsr}$ derived from the spherical approximation. The disk potential sets the circular velocity of the Milky Way that arises from non-dark matter, *i.e.* visible matter.

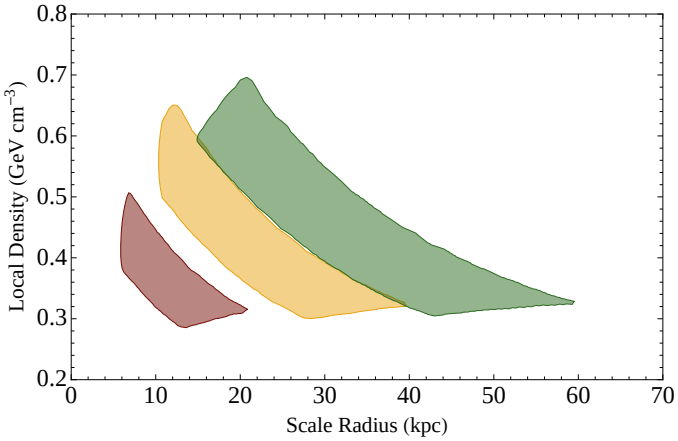

FIG. 1: Region of parameter space in local density (defined at 8.5 kpc) and scale radius, r_s, consistent with (i) halo mass internal to 60 kpc in the range $(4 \pm 0.7) \times 10^{11}$ M$_\odot$, (ii) escape velocity in the range 450-600 km s^{-1}, and (iii) circular velocity in the range 200-280 km s^{-1}, for models with $\alpha = 1$ and $\gamma = 3$ (red), 4 (yellow), and 5 (green).

The measured values of $v_{\rm lsr}$, $v_{\rm esc}$, and the integrated halo mass provide constraints on the parameters of the velocity distribution function. The circular velocity is in the range [32]

$$v_{\rm lsr} = [200, 280] \text{ km s}^{-1}. \tag{17}$$

The 90% confidence level on the escape velocity is in the range

$$v_{\rm esc} = [498, 608] \text{ km s}^{-1}, \tag{18}$$

and is determined from local high velocity stars by the RAVE survey [33]. This constraint on the escape velocity is only attainable for a prior on the spectral index for the velocity distribution of halo stars,

$$f_\star(v) \propto (v_{\rm esc} - v)^{k_\star}, \tag{19}$$

with

$$k_\star = [2.7, 4.7]. \tag{20}$$

Simulations indicate that the power-law index for halo stars is steeper than dark matter. The values of $k_\star$ in (20) correspond to $k = [0.5, 2.5]$ for dark matter [33]. The lower values of k correspond to unphysical halos,

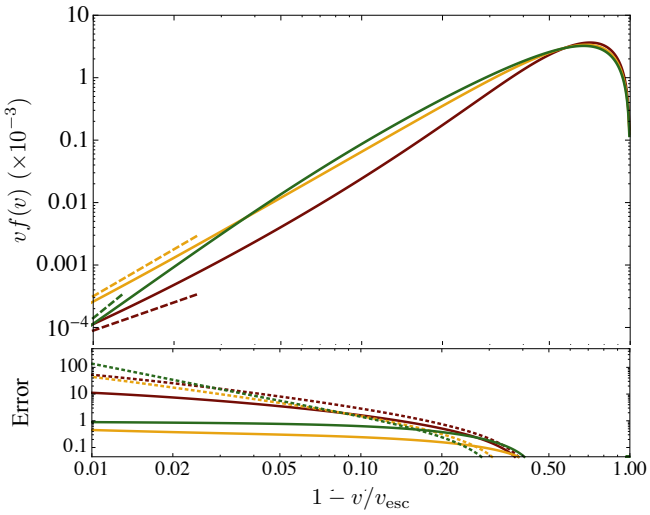

FIG. 2: Distribution functions for models with $\alpha = 1$ and $\gamma = 3$ (red), 4 (yellow), and 5 (green) obtained by numerically solving the Eddington equation with a disk potential as in (16). The dashed lines have slopes of $\gamma - 3/2$. The bottom panel shows the error of using the ansatz velocity distribution (solid) or the King model (dotted) instead of the complete numerical solution.

with $k_\star$ near the lower end of the range in (20). Because the escape velocity is correlated with the spectral index of the stars and the dark matter, if values of k and $k_\star$ on the lower end of the allowed region are used, lower values of $v_{\rm esc}$ must be used, *i.e.* $v_{\rm esc} \simeq [450, 550]$ km s^{-1}.

Finally, there is a bound on the integrated dark matter mass of the Milky Way halo within 60 kpc, determined by distant halo stars to be [34, 35]

$$M(< 60\,{\rm kpc}) = (4.0 \pm 0.7) \times 10^{11} M_\odot. \qquad (21)$$

In the ΛCDM model, an extrapolation of the mass profile to larger radii implies a total Milky Way halo mass of $\sim 10^{12}$ M$_\odot$ [34, 36]. The above constraints are examined in the context of the power-law parameterization in (4); more generic halo profiles are beyond the scope of this analysis, see [37] for further discussion.

Fig. 1 shows the regime of scale radius-local dark matter density parameter space that is consistent with the observational bounds above, where the local dark matter density is simply defined as $\rho(r = 8.5\,{\rm kpc})$ in (4). Three different halo models are shown with different values of the outer slope of $\gamma = 3, 4, 5$. The inner slope is set in all cases to $\alpha = 1$. The implied local density of dark matter is similar for each value of γ, and a larger scale radius is attained for steeper outer density slopes. This scaling of r_0 with γ is ultimately a reflection of the fact that the ratio of the escape velocity to the LSR velocity is bound to be $2.0 \lesssim v_{\rm esc}/v_{\rm lsr} \lesssim 3.5$.

Fig. 2 shows velocity distributions, $vf(v)$, as a function of $1 - v/v_{\rm esc}$ resulting from the numerical solution of the Eddington inversion formula for the three density models with outer slopes of $\gamma = 3, 4, 5$ using the regions delineated in Fig. 1. In particular, the local density is set at 0.27 GeV cm^{-3} and $r_s = 20, 28, 37$ kpc for $\alpha = 1$ and $\gamma = 3, 4, 5$, respectively. The disk and bulge potential are included in the gravitational potential. The numerical evaluation of the Eddington formula extends over a wide enough range to ensure that the velocity distribution function is convergent; in practice, this requires that the potential goes to zero at $r \gtrsim 100 r_s$. Tangent curves show the analytic behavior of the outer slopes. The inclusion of the disk component does not alter the behavior at small $1 - v/v_{\rm esc}$. The bottom panel of Fig. 2 shows the error of using the ansatz velocity distribution function of (1) or the King model instead of the full numerical solution of the Eddington equation, $f_{\rm E}(v)$. The error is defined as

$$\text{Error} = \left| \frac{f_k(v) - f_{\rm E}(v)}{f_{\rm E}(v)} \right|. \qquad (22)$$

The agreement between the power-law slope and the numerical calculation is the best for the density models with the steepest outer slopes, while numerical calculation for the NFW model with outer slope behavior of r^{-3} has a slightly steeper slope than $k = 1.5$. For the NFW, this is a reflection of the fact that the tail of the distribution is modified, so that as $\mathcal{E} \to 0$, the distribution function scales as

$$f(\mathcal{E}) \to \frac{\mathcal{E}^{\frac{3}{2}}}{(-\ln \mathcal{E})^3}, \qquad (23)$$

rather than as a pure power-law in $\mathcal{E}$ [14]. The behavior near $\mathcal{E} = 0$ is steeper than a $k = \frac{3}{2}$ power-law and $k_{\rm NFW} \simeq 2.0$ typically fits better numerically.

B. Comparison to Simulated Galactic Halos

High resolution simulations of Galactic halos with dark matter only have revealed a non-Maxwellian structure to velocity distributions [6, 7]. Several trends are seen in these simulations. The low velocity tail is more populated than the best fitting Maxwellian distribution, while the peak is more depressed. At moderately high velocities beyond the peak, the distribution is more populated than the best fitting Maxwellian. Further, broad bumps that represent dynamical features are prevalent in the velocity modulus distribution, though they are not present in the distribution of the individual velocity components. Although features in the distribution due to substructure are present at some locations in the halo, their contribution to the velocity distribution averaged over all radial shells is typically sub-dominant relative to the broader bumps. The highest resolution simulation in the literature that includes baryonic physics [8] does not show such features, and is better described by a Maxwellian distribution than the dark matter only simulations, though it still deviates at the high velocity tail. It remains to be

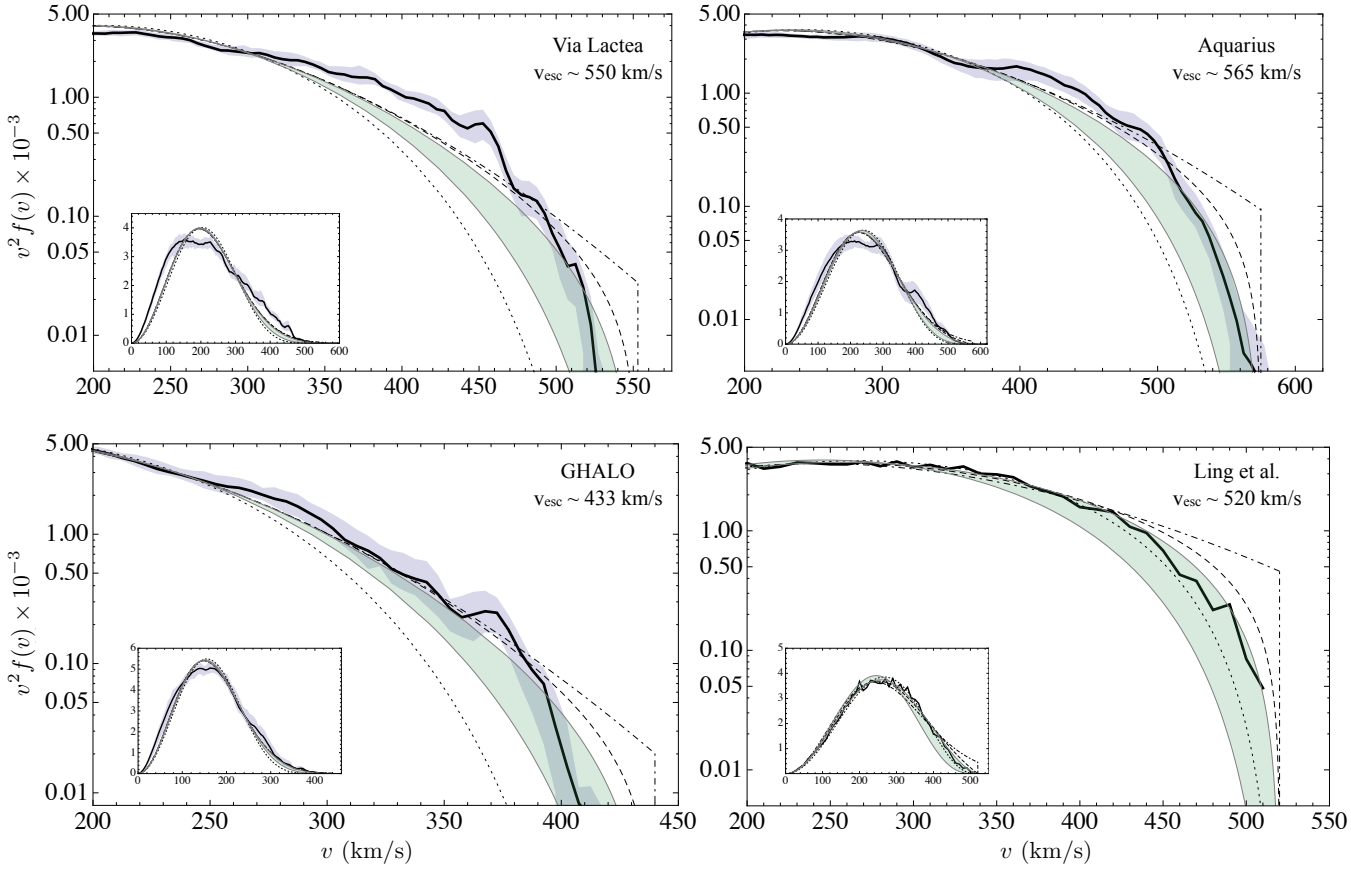

FIG. 3: Best-fit Maxwellian (dot-dashed), King (dashed), and Tsallis (dotted) models to the Via Lactea, Aquarius, GHALO, and Ling et al. [8] simulations (solid black). The first three are simulated with dark matter only; [8] simulates a galaxy with baryons. The green band shows the velocity distribution obtained by fitting (1) to the data for $1.5 < k < 3.5$. The purple shaded regions enclose 68% of all measured distributions in each of the Aquarius, Via Lactea, and GHALO panels.

seen whether this result is robust to changes in uncertain baryonic physics and scatter in formation histories between galaxies.

The features of these velocity distributions clearly reflect the formation process of each individual halo, and deviate from sphericity and isotropy in both the density distributions and velocity ellipsoids. Of course, they also reflect the distribution of the individual dark matter halo that was simulated, and it is not yet known how this quantity in individual halos relates to the distribution of the velocity distribution for a larger sample of similar mass halos. Further, it is also assumed that the velocity distributions from numerical simulations provide an unbiased tracer of the velocity distribution of the actual Milky Way dark halo. This latter point can be addressed by choosing simulated halos to have a mass and isolation criteria that resemble the Milky Way regime. These selection criteria could be further refined by demanding additional constraints, *e.g.*, requiring a similar number of massive, Magellanic cloud-like satellites to the Milky Way [38]. In spite of these caveats, comparisons to N-body simulations are still critical for determining how well analytic arguments based upon the assumption of equilibrium match typical galaxies.

Fig. 3 shows the best fits of the velocity distribution function from (1) to the results of the Aquarius, Via Lactea II, and GHALO dark matter only simulations, and the simulation with baryons of Ling et al. [8]. The high energy tails are shown in the main figures in each of the four panels while the insets show the fits to the full velocity distribution function. The shaded bands in this figure represent slopes in the range $k = [1.5, 3.5]$, corresponding to outer slopes between $\gamma = [3.0, 5.0]$. For each value of k within this band, the parameter v_0 has been fit to the distribution, and $v_{\rm esc}$ is set to the value determined by each of the respective simulations. Implicit in this assumption is that the highest velocity particle is a faithful tracer of $v_{\rm esc}$, rather than a contaminating particle that is not bound to the halo.

The best-fit SHM, King, and Tsallis distributions are shown for comparison in all panels of Fig. 3. In all panels, the SHM does not go to zero smoothly at the escape velocity, indicating that this distribution function is unphysical in the tail. By construction, the velocity distribution in (1) smoothly joins to a Maxwellian distribution for any value of k, with the differences manifest only near

the tails.

The fits shown in Fig. 3 indicate that the velocity distribution in (1) captures the high velocity tail of the simulated distribution well, especially in comparison to the King, SHM, and Tsallis distributions. This is in spite of the fact that the simulations are clearly anisotropic and non-spherical, and that the outer regimes of the halo may not have fully equilibrated. The agreement demonstrated in Fig. 3 is promising, though larger samples of dark matter halos at similar resolution are needed to verify the high velocity suppression that (1) predicts. Consistent with previous findings, the dark matter only simulations are more 'flat-topped' than all of the models, while there are more particles in the low regime of the velocity distribution. The enhancement of low velocity particles may result from radially-biassed anisotropy, as discussed below. The Ling et al. [8] distribution best resembles a Maxwellian profile at low velocities. This agreement might be attributed to either the effect of baryonic physics, which has been shown to result in more isotropic inner halos [39], or to the lower resolution of dark matter simulations that include baryons.

A final point regarding the comparison to the simulations is that, since the tail appears well described by $k = [1.5, 3.5]$, it is plausible to conjecture that baryons do not appear to greatly affect the shape of the velocity distribution near the escape velocity. One way to understand this is that since highly energetic particles with large peri-center orbits shape the tail of the distributions, these dark matter particles will be outside the halo's scale radius for a large fraction of their orbits. The scale radius ranges between $r_s \simeq [10, 60]$ kpc (see Fig. 1) for the models considered, and the Galactic disk is located in the regime where the density scales as the inner slope, α. The inner slope should not significantly perturb the orbits of the halo's most energetic particles that make up the high velocity tail. Thus, the regime most likely to be affected by the formation of the disk are the orbits in the the inner core of the halo, where the power-law depends on α.

IV. DIRECT DETECTION

The velocity distribution function in (1) reproduces the results from N-body simulations and exhibits non-Gaussian behavior near the escape velocity. This section shows that the suppression in the high energy tail has important implications for the interpretation of direct detection experiments.

The scattering rate of a dark matter particle off a target nucleus depends on the velocity-averaged differential cross section and is thus sensitive to the distribution function. The detection rate per unit detector mass is

$$\frac{dR_k}{dE_R} = \frac{\rho_0}{m_{\rm dm} m_N} \int_{v_{\rm min}}^{v_{\rm esc}} d^3v \; f_k(\vec{v} + \vec{v}_E(t)) v \frac{d\sigma}{dE_R}, \quad (24)$$

where m_N is the mass of the target nucleus, $m_{\rm dm}$ is the dark matter mass, μ_N is the reduced mass of the nucleus-dark matter system, E_R is the nuclear recoil energy, ρ_0 is the local dark matter density, and $f_k(\vec{v} + \vec{v}_E(t))$ is the velocity distribution function in the Earth's rest frame with a power-law index, k [21, 40]. The spin-independent differential cross section is parameterized as

$$\frac{d\sigma}{dE_R} = \frac{m_N \sigma_n}{2\mu_n^2 v^2} (f_p Z + f_n (A - Z))^2 |F_N(q^2)|^2, \quad (25)$$

where σ_n is the dark matter-nucleon cross section at zero momentum transfer, μ_n is the dark matter-nucleon reduced mass, and $q^2 = 2 m_N E_R$ is the momentum transfer. $f_{p,n}$ parameterize the coupling to the proton and neutron and are typically set to unity. $F_N(q^2)$ is the nuclear form factor, for which the Helm/Lewin-Smith form is used [21].

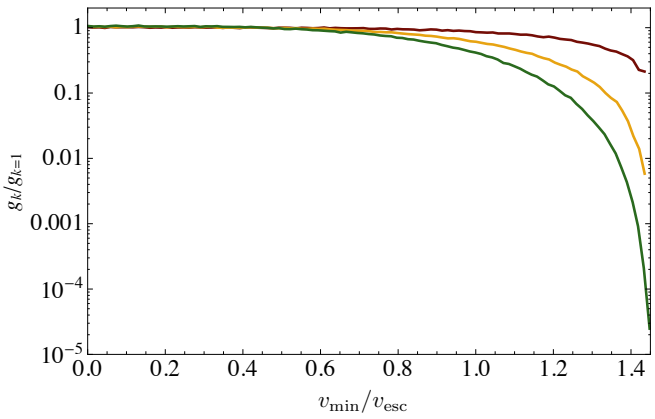

FIG. 4: Fractional change in the differential dark matter detection rate as a function of the minimum velocity for $k = 1.5$ (red), 2.5 (yellow), and 3.5 (green), compared to a King velocity distribution function with $k = 1$. In this figure, $v_0 = 220$ km/s, $v_{\rm esc} = 550$ km/s, and the Earth's velocity is taken at $\sim$ June 2.

The relevant quantity when comparing direct detection rates for velocity distributions with different spectral indices is

$$g_k(v_{\rm min}) = \int_{v_{\rm min}}^{v_{\rm esc}} dv \;\; v \, f_k(\vec{v} + \vec{v}_E(t)). \quad (26)$$

The ratio g_k/g_1 illustrates how the new *ansatz* compares with the more commonly used King model. In the limit where $v_{\rm min} \to 0$, the ratio g_k/g_1 approaches unity for properly normalized distributions. However, this ratio deviates from unity when the minimum scattering velocity is $\sim 60\%$ of the escape velocity, as illustrated in Fig. 4. As the minimum velocity approaches the maximum dark matter velocity, $v_{\rm esc} + v_E(t)$, the scattering rate is strongly suppressed. This suppression can be as large as two orders of magnitude for an outer slope of $\gamma = 4$, or five orders of magnitude for $\gamma = 5$.

Dark matter with particularly large minimum scattering velocities will be most sensitive to increases in the

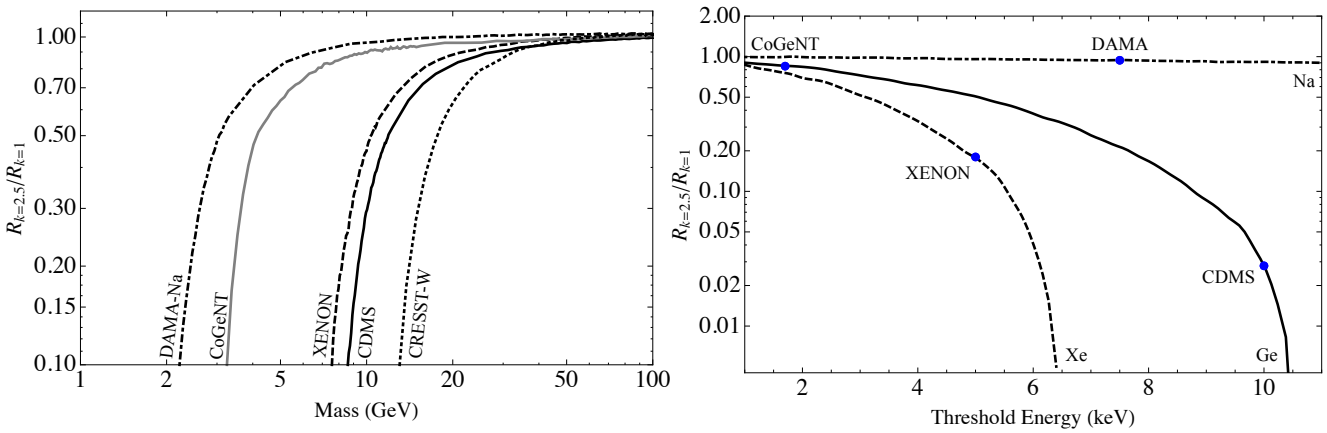

FIG. 5: Fractional change in the scattering rate for $k = 2.5$ compared to $k = 1$ for an elastically scattering dark matter with $v_0 = 220$ and $v_{\rm esc} = 550$ km/s. The plot on the left illustrates the dependence of the scattering rate on the dark matter mass for DAMA-Na (dot-dashed) [43], CoGeNT (solid gray) [44], XENON (dashed) [45, 46], CDMS (solid black) [47], and CRESST-W (dotted) [48] for threshold energies of 7.5, 1.7, 5, 10, and 10 keV, respectively. The plot on the right illustrates the dependence of the scattering rate on the threshold energy for an 8 GeV dark matter scattering elastically off a Xe (dashed), Ge (solid), and Na (dot-dashed) target. In both plots, the Earth's velocity was taken at $\sim$ June 2.

spectral index of the velocity distribution function. The minimum velocity depends on the kinematics of the scattering event and is given by

$$v_{\rm min} = \frac{1}{\sqrt{2 m_N E_R}} \Big(\frac{m_N E_R}{\mu_N} + \delta \Big), \qquad (27)$$

where δ is the mass splitting between the initial and final dark matter states if dark matter scattering is dominantly inelastic; elastic scattering corresponds to $\delta = 0$. Figure 4 shows the effect of the power-law index k on the direct detection rate, as a function of $v_{\rm min}$.

Inelastic dark matter [41] is sensitive to the spectral index of the distribution function because it has a larger $v_{\rm min}$. The minimum scattering velocity differs between experiments with different energy thresholds or target nuclei. As a result, a change in the spectral index of the velocity distribution affects the limits for each experiment differently. For example, an experiment with a heavier target nucleus or a lower threshold energy will have a fairly large value for $v_{\rm min}$ and a greater sensitivity to the velocity distribution function.

Light elastic dark matter is also sensitive to the high velocity tail of Galactic dark matter [42]. Fig. 5 illustrates the suppression of the scattering rate R_k (integrated over recoil energy) relative to that for the King model. For example, if $m_{\rm dm} = 8\,{\rm GeV}$, a Xe target with 5 keV threshold energy has $R_{2.5}/R_1 \simeq 0.18$. This ratio is more suppressed as one goes to heavier target nuclei and/or larger threshold energy. For instance, a Ge target with $E_{\rm th} = 10\,{\rm keV}$ is suppressed relative a Ge target with a $E_{\rm th} = 2\,{\rm keV}$ by a factor of 25. In the case of light target nuclei (i.e., Na), or low threshold energies (i.e., $\lesssim 2\,{\rm keV}$), the effect of increasing the spectral index is much less significant, with $R_{2.5}/R_1 \sim 1$. The relative changes in the rates have profound consequences when comparing a potential signal in one experiment with the result of another experiment with a different target nucleus or threshold energy.

V. DISCUSSION AND CONCLUSION

This paper has considered a cosmologically-motivated class of double power-law dark matter density profiles and has examined the resulting velocity distribution, assuming isotropy and spherical symmetry. This article has specifically focused on the behavior of the velocity distribution at low binding energies, near the escape velocity. The primary result is that the velocity distribution function is well-modeled by the function presented in (1), where the power-law index ,k, is in the range ~ 2. This is a steeper fall-off than what is expected for a Maxwell-Boltzmann distribution, which has served as the canonical model for dark matter velocity distributions in the recent literature. The new ansatz in (1) affects the interpretation of limits set by direct dark matter detection experiments. Limits on low mass dark matter, $m_{\rm dm} \lesssim 40\,{\rm GeV}$, are most strongly affected, especially for experiments with heavy target nuclei or large threshold energies.

The analysis presented in this article does not address the effects of anisotropy and deviations from spherical symmetry, which are expected to be more serious in the outskirts of the profile most relevant for the high velocity tail [49]. For instance, anisotropy could be responsible for $\alpha \ll 2$. For anisotropic distributions, there is no guarantee that a given density distribution will correspond to a unique distribution function. For example, if the distribution function is deformed to $L^{-2\beta} f(\mathcal{E})$, the distribution function depends only on a single derivative of

the density with respect to the potential for radial orbits of $\beta = \frac{1}{2}$ [15]. The corresponding velocity distribution scales as $f(v) \propto v$ at low velocities, which is broadly consistent with the behavior in the dark matter only simulations of Fig. 3. In comparison, the low velocity behavior of the Galactic halo for a circularly biased system with $\beta = -\frac{1}{2}$ is $f(v) \propto v^3$. Thus, the low energy tail may indicate the presence of radial orbits in the halos, which would be consistent with the velocity anisotropy distribution in numerical simulations [50].

The interplay between density profiles of dark matter halos and their corresponding velocity distribution functions was developed in this paper, but requires further study. Exploring equilibrium dark matter phase space distributions, particularly anisotropic distributions, may give further insight into the behavior of N-body simulations and may explain the inner slope of $\rho(r)$. These effects are unlikely to be directly observable in early direct detection experiments, but may be seen in future directional dark matter detection experiments [51].

Acknowledgments

We thank Sonia El-Hedri and Daniele Alves for enlightening discussions on the behavior of Maxwell-Boltzmann-like distributions at large and small radii. We thank Patrick Fox, Jeremiah Ostriker, David Spergel, and Neal Weiner for useful discussions. We additionally thank Michael Kuhlen, Fu-Sin Ling, and Mark Vogelsberger for providing numerical files used in Fig. 3. JGW and RHW are supported by the DOE under contract DE-AC03-76SF00515. JGW is partially supported by the DOE's Outstanding Junior Investigator Award and the Sloan Foundation. LES acknowledges support for this work from NASA through Hubble Fellowship grant HF-01225.01 awarded by the Space Telescope Science Institute, which is operated by the Association of Universities for Research in Astronomy, Inc., for NASA, under contract NAS 5-26555. ML acknowledges support from the Simons Postdoctoral Fellows Program and the LHC Theory Initiative. Lastly, we acknowledge the second sphenic number for inspiration.

[1] J. F. Navarro, C. S. Frenk and S. D. M. White, Astrophys. J. **490**, 493 (1997) [arXiv:astro-ph/9611107]; J. F. Navarro *et al.*, arXiv:0810.1522 [astro-ph]; J. Stadel, D. Potter, B. Moore *et al.*, [arXiv:0808.2981 [astro-ph]].
[2] A. S. Eddington, MNRAS **76**, 572 (1916).
[3] J. Binney and S. Tremaine. *Galactic Dynamics*. Princeton: Princeton University Press, 2008.
[4] A. K. Drukier, K. Freese, D. N. Spergel, Phys. Rev. **D33**, 3495-3508 (1986); K. Freese, J. A. Frieman, A. Gould, Phys. Rev. **D37**, 3388 (1988).
[5] C. Savage, K. Freese, P. Gondolo and D. Spolyar, JCAP **0909**, 036 (2009) [arXiv:0901.2713 [astro-ph]]; A. M. Green, arXiv:1009.0916 [astro-ph.CO]; P. Belli, R. Cerulli, N. Fornengo *et al.*, Phys. Rev. **D66**, 043503 (2002). [hep-ph/0203242].
[6] M. Vogelsberger *et al.*, Mon. Not. Roy. Astron. Soc. **395**, 797 (2009) [arXiv:0812.0362 [astro-ph]].
[7] M. Kuhlen *et al.*, JCAP **1002**, 030 (2010) [arXiv:0912.2358 [astro-ph.GA]].
[8] F. S. Ling, E. Nezri, E. Athanassoula and R. Teyssier, JCAP **1002**, 012 (2010) [arXiv:0909.2028 [astro-ph.GA]].
[9] M. Fairbairn and T. Schwetz, JCAP **0901**, 037 (2009) [arXiv:0808.0704 [hep-ph]].
[10] P. J. T. Leonard and S. Tremaine, Astrophys. J. **353**, 486 (1990).
[11] J. Hjorth, L. L. R. Williams, Astrophys. J. **722**, 851-855 (2010). [arXiv:1010.0265 [astro-ph.CO]]; L. L. R. Williams, J. Hjorth, R. Wojtak, [arXiv:1010.0267 [astro-ph.CO]]; L. L. R. Williams, J. Hjorth, Astrophys. J. **722**, 856-861 (2010). [arXiv:1010.0266 [astro-ph.CO]].
[12] S. Chaudhury, P. Bhattacharjee, R. Cowsik, JCAP **1009**, 020 (2010). [arXiv:1006.5588 [astro-ph.CO]].
[13] S. H. Hansen, D. Egli, L. Hollenstein and C. Salzmann, New Astron. **10**, 379 (2005) [arXiv:astro-ph/0407111].
[14] L. M. Widrow, ApJ&S, **131**, 39 (2000)
[15] N. W. Evans and J. H. An, Phys. Rev. D **73**, 023524 (2006) [arXiv:astro-ph/0511687].
[16] E. L. Lokas and G. A. Mamon, Mon. Not. Roy. Astron. Soc. **321**, 155 (2001) [arXiv:astro-ph/0002395]; P. Ullio and M. Kamionkowski, JHEP **0103**, 049 (2001) [arXiv:hep-ph/0006183]; S. Kazantzidis, J. Magorrian, B. Moore, Astrophys. J. **601**, 37-46 (2004). [astro-ph/0309517]; S. H. Hansen, Mon. Not. Roy. Astron. Soc. **352**, L41 (2004). [astro-ph/0405371]; C. G. Austin, L. L. R. Williams, E. I. Barnes *et al.*, Astrophys. J. **634**, 756-774 (2005). [astro-ph/0506571]. S. H. Hansen, Astrophys. J. **694**, 1250-1255 (2009). [arXiv:0812.1048 [astro-ph]]; J. D. Vergados and D. Owen, Phys. Rev. D **75**, 043503 (2007) [arXiv:astro-ph/0603704].
[17] A. Helmi, S. D. M. White and V. Springel, Phys. Rev. D **66**, 063502 (2002) [arXiv:astro-ph/0201289].
[18] D. Stiff and L. M. Widrow, Phys. Rev. Lett. **90**, 211301 (2003) [arXiv:astro-ph/0301301].
[19] M. Kamionkowski and S. M. Koushiappas, Phys. Rev. D **77**, 103509 (2008) [arXiv:0801.3269 [astro-ph]].
[20] A. H. G. Peter, Phys. Rev. **D79**, 103533 (2009); [arXiv:0902.1348 [astro-ph.HE]]. J. Edsjo, A. H. G. Peter, [arXiv:1004.5258 [astro-ph.EP]].
[21] J. D. Lewin and P. F. Smith, Astropart. Phys. **6**, 87 (1996).
[22] R. H. Wechsler, J. S. Bullock, J. R. Primack *et al.*, Astrophys. J. **568**, 52-70 (2002). [astro-ph/0108151]; D. Zhao,

H. Mo, Y. Jing *et al.*, Mon. Not. Roy. Astron. Soc. **339**, 12-24 (2003). [astro-ph/0204108].

[23] J. Wang, S. D. M. White, Mon. Not. Roy. Astron. Soc. **396**, 709-717 (2009) [arXiv:0809.1322 [astro-ph]].

[24] D. Lynden-Bell, Mon. Not. Roy. Astron. Soc. **136** (1967) 101.

[25] L. Hernquist, Astrophys. J. **356**, 359 (1990).

[26] M. Kamionkowski and A. Kinkhabwala, Phys. Rev. D **57**, 3256 (1998) [arXiv:hep-ph/9710337].

[27] C. S. Kochanek, Astrophys. J. **457**, 228 (1996) [astro-ph/9505068].

[28] S. D. Tremaine, I.A.U.Symp.**127**, ed. T. de Zeeuw (Dordrecht: Reidel) 367, 1987.

[29] M. T. Busha, A. E. Evrard, F. C. Adams *et al.*, Mon. Not. Roy. Astron. Soc. Lett. **363**, L11-L15 (2005). [astro-ph/0412161].

[30] S. H. Hansen, B. Moore, M. Zemp *et al.*, JCAP **0601**, 014 (2006) [astro-ph/0505420].

[31] M. Maciejewski, M. Vogelsberger, S. D. M. White *et al.*, [arXiv:1010.2491 [astro-ph.CO]].

[32] M. J. Reid *et al.*, Astrophys. J. **700**, 137 (2009) [arXiv:0902.3913 [astro-ph.GA]]; J. Bovy, D. W. Hogg and H. W. Rix, Astrophys. J. **704**, 1704 (2009) [arXiv:0907.5423 [astro-ph.GA]]; P. J. McMillan and J. J. Binney, arXiv:0907.4685 [astro-ph.GA].

[33] M. C. Smith *et al.*, Mon. Not. Roy. Astron. Soc. **379**, 755 (2007) [arXiv:astro-ph/0611671].

[34] X. X. Xue *et al.* [SDSS Collaboration], Astrophys. J. **684**, 1143 (2008) [arXiv:0801.1232 [astro-ph]].

[35] O. Y. Gnedin, W. R. Brown, M. J. Geller *et al.*, Astrophys. J. **720**, L108 (2010). [arXiv:1005.2619 [astro-ph.GA]]; W. R. Brown, M. J. Geller, S. J. Kenyon *et al.*, [arXiv:0910.2242 [astro-ph.GA]].

[36] Y. S. Li and S. D. M. White, Mon. Not. Roy. Astron. Soc. **384**, 1459 (2008) [arXiv:0710.3740 [astro-ph]].

[37] W. Dehnen and J. Binney, Mon. Not. Roy. Astron. Soc. **294**, 429 (1998) [arXiv:astro-ph/9612059]; A. M. Green, JCAP **0807**, 005 (2008) [arXiv:0805.1704 [hep-ph]]; L. E. Strigari and R. Trotta, JCAP **0911**, 019 (2009) [arXiv:0906.5361 [astro-ph.HE]]; R. Catena and P. Ullio, JCAP **1008**, 004 (2010) [arXiv:0907.0018 [astro-ph.CO]]; A. H. G. Peter, Phys. Rev. D **81**, 083511 (2010) [arXiv:1001.3870 [astro-ph.CO]]; C. McCabe, Phys. Rev. D **82**, 023530 (2010) [arXiv:1005.0579 [hep-ph]]; M. Pato, O. Agertz, G. Bertone *et al.*, Phys. Rev. **D82**, 023531 (2010) [arXiv:1006.1322 [astro-ph.HE]].

[38] M. T Busha, P Marshall, and R. H. Wechsler, ApJL, to be submitted.

[39] S. Kazantzidis, A. V. Kravtsov, A. R. Zentner *et al.*, Astrophys. J. **611**, L73-L76 (2004). [astro-ph/0405189]; R. A. Flores, B. Allgood, A. V. Kravtsov *et al.*, Mon. Not. Roy. Astron. Soc. **377**, 883-896 (2007). [astro-ph/0508226].

[40] R. Schoenrich, J. Binney, W. Dehnen, [arXiv:0912.3693 [astro-ph.GA]]

[41] D. Tucker-Smith, N. Weiner, Phys. Rev. **D64**, 043502 (2001). [hep-ph/0101138]; S. Chang, G. D. Kribs, D. Tucker-Smith *et al.*, Phys. Rev. **D79**, 043513 (2009). [arXiv:0807.2250 [hep-ph]]; D. S. M. Alves, M. Lisanti, J. G. Wacker, Phys. Rev. **D82**, 031901 (2010). [arXiv:1005.5421 [hep-ph]].

[42] F. Petriello, K. M. Zurek, JHEP **0809**, 047 (2008). [arXiv:0806.3989 [hep-ph]]; D. E. Kaplan, M. A. Luty, K. M. Zurek, Phys. Rev. **D79**, 115016 (2009). [arXiv:0901.4117 [hep-ph]]; A. L. Fitzpatrick, D. Hooper, K. M. Zurek, Phys. Rev. **D81**, 115005 (2010). [arXiv:1003.0014 [hep-ph]]; S. Chang, J. Liu, A. Pierce *et al.*, JCAP **1008**, 018 (2010). [arXiv:1004.0697 [hep-ph]].

[43] R. Bernabei *et al.* [DAMA], Int. J. Mod. Phys. D **13**, 2127 (2004) [arXiv:astro-ph/0501412]. R. Bernabei *et al.* [DAMA], Eur. Phys. J. C **56**, 333 (2008) [arXiv:0804.2741 [astro-ph]]; R. Bernabei, P. Belli, F. Cappella *et al.*, Eur. Phys. J. **C67**, 39-49 (2010) [arXiv:1002.1028 [astro-ph.GA]].

[44] C. E. Aalseth *et al.* [CoGeNT Collaboration], [arXiv:1002.4703 [astro-ph.CO]].

[45] E. Aprile *et al.* [XENON100], [arXiv:1005.0380 [astro-ph.CO]].

[46] J. Angle *et al.*, [XENON10], arXiv:0910.3698 [astro-ph.CO].

[47] D. S. Akerib *et al.* [CDMS], Phys. Rev. D **73**, 011102 (2006) [arXiv:astro-ph/0509269]; D. S. Akerib *et al.* [CDMS], Phys. Rev. Lett. **96**, 011302 (2006) [arXiv:astro-ph/0509259]; Z. Ahmed *et al.* [CDMS], arXiv:0802.3530 [astro-ph]; Z. Ahmed *et al.* [CDMS II], *Science* **327**, 1619 (2010) [arXiv:0912.3592 [hep-ph]].

[48] G. Angloher *et al.*[CRESST], Astropart. Phys. **23**, 325 (2005) [arXiv:astro-ph/0408006]. G. Angloher *et al.*[CRESST], arXiv:0809.1829 [astro-ph].

[49] B. Allgood, R. A. Flores, J. R. Primack *et al.*, Mon. Not. Roy. Astron. Soc. **367**, 1781-1796 (2006). [astro-ph/0508497].

[50] S. H. Hansen and B. Moore, New Astron. **11**, 333 (2006) [arXiv:astro-ph/0411473].

[51] O. Host and S. H. Hansen, JCAP **0706**, 016 (2007) [arXiv:0704.2909 [astro-ph]].